

Experiments in Imaging Early Aftershocks of Large Earthquakes

Award 05HQGR0099

Peter M. Shearer
Institute of Geophysics and Planetary Physics
Scripps Institution of Oceanography
University of California, San Diego
La Jolla, CA 92093
858-534-2260 (phone), 858-534-5332 (fax)
pshearer@ucsd.edu

Key words: Seismology, Seismotectonics, Source Characteristics

Annual Project Summary

Investigations Undertaken

In consultation with National Earthquake Information Center (NEIC) researchers, we are investigating practical methods to routinely detect and image very early aftershocks of large earthquakes. Our work so far has focused on the 22 December 2003 Mw 6.5 San Simeon earthquake. Our method uses a matched-filter technique to back-project energy to the source region in order to image finite-source effects and locate early aftershocks that may be hidden in the coda of the mainshock. Our goal is to develop a method that can be implemented in real time that provides approximate aftershock locations and can be used to quickly identify the primary fault plane and the rupture propagation direction, information that can improve the rapid calculation of strong ground-motion predictions.

Results

Recently, we have shown that back-projection of teleseismic P waves can be used to directly image the rupture extent of large earthquakes (Ishii et al., 2005; Walker et al., 2005). We are currently working to implement an operational version of our algorithms at the NEIC in order to provide fault rupture images to researchers within 20 to 30 minutes following earthquake initiation. This will make possible the release of more timely estimates regarding where the strongest shaking is likely to have occurred and the probability of tsunami generation.

The back-projection method

Our back-projection method is a simplification of wavefield reverse-time migration, a tool for imaging structure in reflection seismology. For the j th source location, the seismograms are summed to make the stack s_j as a function of time t :

$$s_j(t) = \sum_k (p_k/A_k) u_k(t - t_{jk}^P + \Delta t_k),$$

where $u_k(t)$ is the vertical-component seismogram recorded at the k th station, and t_{jk}^P is the theoretical P -wave travel time from the j th source to the k th station (currently computed using the IASP91 velocity model). Δt_k denotes timing corrections obtained from waveform cross-correlation of the initial part of the P waves, which are used to enhance the coherence of the traces by accounting for effects due to 3-D structure. Finally, p_k and A_k are the polarity and amplitude of the seismograms obtained through cross-correlation analysis; the division by A_k insures that the traces have approximately equal weight. The stacking procedure sums the energy that is radiated from the given source point constructively and attenuates other energy present in the seismograms.

Filtering can be applied to the seismograms to enhance certain frequency bands but acceptable results are often obtained with simple demeaning of the traces. To ensure waveform similarity, only seismograms with a correlation coefficient for the initial *P*-wave of greater than a threshold value (typically 0.7) with respect to a waveform stack are included in the analysis. Starting windows for the cross-correlation are obtained using either predicted *P* arrival times or picks from an automatic picking algorithm (Earle and Shearer, 1994). The stacking is performed over an evenly spaced grid of source latitude and longitude, assuming a constant source depth. No prior assumptions are made regarding fault geometry. Differences in expected amplitudes from geometrical spreading, source depth variations and directivity effects are ignored, but they should be relatively minor.

The spatial resolution depends upon the array geometry and the frequency content of the data but typically is 50 to 150 km. The stack coherence is greatest close to the hypocenter and will deteriorate at more distant source imaging points where the 3-D velocity structure along the ray paths differs from that at the hypocenter. Despite this effect, the method successfully images the 2004 Sumatra-Andaman rupture, which extends over 1000 km from its hypocenter. Enhanced coherence at different rupture imaging points can, in principle, also be improved by performing waveform cross-correlation on aftershocks to obtain additional sets of empirical timing corrections. However, because aftershock occurrence is not immediate this approach is less suited to real-time applications than using 3-D velocity models.

The 26 December 2004 Sumatra-Andaman earthquake

The disastrous Sumatra-Andaman earthquake of December 26, 2004 was one of the largest ever recorded and generated a tsunami that killed hundreds of thousands of people. However, prediction of the tsunami was hampered by delays in recognizing the true magnitude and extent of the fault rupture. The initial NEIC body wave magnitude (determined automatically) was only 6.2. An hour later, this was increased to a surface wave magnitude of 8.5. The Harvard CMT solution of $M_w = 8.9$ (later adjusted to 9.0) was provided 6 hours after the earthquake. Clearly there is a need for a method that can quickly measure event size using the initial *P*-wave arrivals, rather than waiting for the slower surface wave arrivals.

The back-projection approach described above is such a method and can produce detailed images within 20 to 30 minutes of rupture initiation. It requires no prior knowledge of fault geometry, dimension, or rupture duration. In addition, this observation-driven method takes advantage of the entire *P* wavetrain and calculation of synthetic seismograms is not needed. It is insensitive to interference with later seismic phases such as *PP*, because their angle of incidence across the array is different from direct *P*. Finally, our approach provides more detailed images of rupture timing and extent than simple measures of short-period *P*-wave duration versus azimuth such as those performed by Ni et al. (2005) for the Sumatran earthquake.

We first tested the method using data from the short-period Hi-Net seismic array in Japan. Our signal-to-noise cutoff resulted in 538 seismograms out of 686 available traces. Figure 1 shows the distribution of cumulative radiated energy in the 600 s from the start of the earthquake. The slip is greatest near the epicenter west of northern Sumatra, but there is also significant radiation in the northern portion west of Nicobar and Andaman Islands. The rupture is not confined to the southern part of the aftershock zone as some of the early finite slip models suggested. By studying the time dependence in these images, we find the rupture spread over the entire 1300-km-long aftershock zone by propagating northward at roughly 2.8 km/s for ~8 minutes. Comparisons with the aftershock areas of other great earthquakes suggest a moment magnitude of ~9.3 for the Sumatran event. Its rupture, in both duration and extent, is the longest ever recorded.

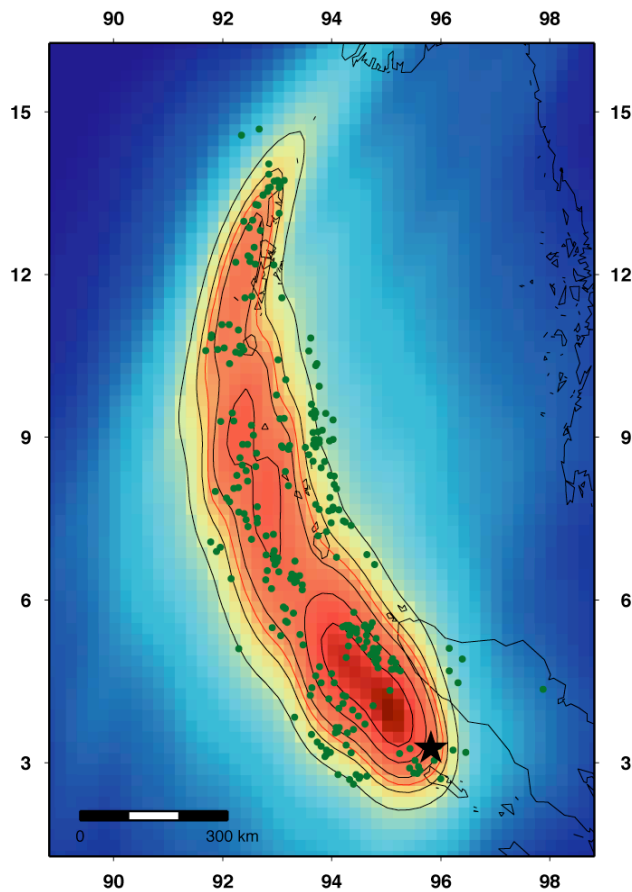


Figure 1. Seismic energy from the Sumatra-Andaman earthquake integrated over 600 seconds after initiation, normalised such that the maximum value is unity. The red contour, plotted at 65% of the maximum, encloses the slip area used to estimate the moment magnitude. The epicenter is shown as the black star. Note the good agreement between the 1300-km-long rupture zone and the locations of the first month of aftershocks (dark green circles). The black contours are plotted at increments of 0.1 starting at 0.5. The image is computed and shown across the entire map but amplitudes are very weak outside the contoured region.

Although the Japanese Hi-Net data provide the best images of this earthquake, useful results can also be obtained for Global Seismic Network (GSN) stations that are available in real time to the NEIC. Figure 2 shows results for the Sumatran earthquake, as obtained both using 112 global distributed stations and 47 stations located in Europe and the Middle East, at distances between 30 and 95 degrees from the hypocenter. We have generally found that superior results are obtained for very large earthquakes by using a regional subset of the global station distribution. Presumably this is a result of greater coherence with respect to 3-D velocity variations as the back-projected image moves away from the hypocenter. It may also involve complications arising from directivity and radiation pattern effects. Regardless, either approach would have quickly shown the roughly 1200-km long northward progression of the rupture from the epicenter within 30 minutes of the start of the Sumatra-Andaman earthquake.

The 28 March 2005 Sumatra earthquake

On March 28, 2005, another thrust event occurred with an estimated M_w of 8.7, about 300 km to the east-southeast of the December 26 earthquake. The surface shaking resulted in at least 2000 casualties, most of which were on the island of Nias about 100 km south-southeast of the hypocenter. This event did not produce a significant tsunami, as might have been expected based on the focal mechanism, which was nearly identical to that of the December M_w 9.3 event. However, this event was the second largest earthquake since the great 1964 Alaska earthquake.

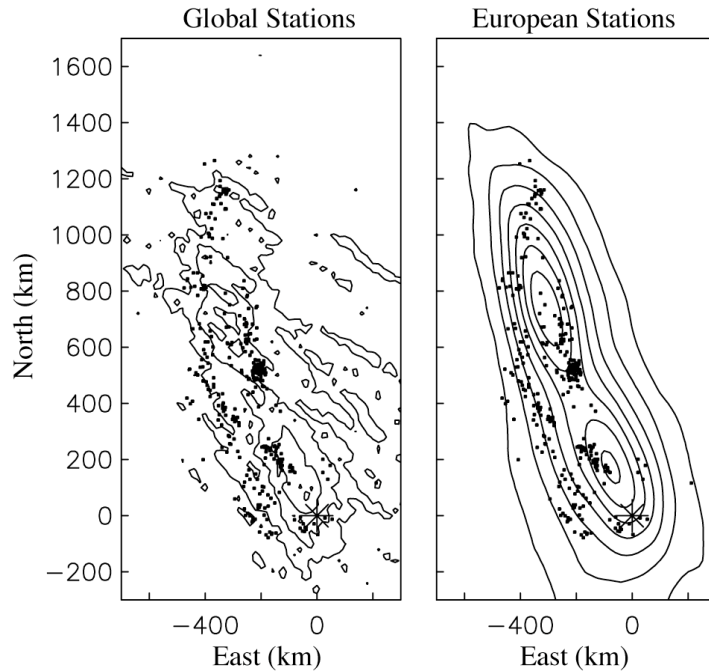


Figure 2. Images of the 2004 Sumatra-Andaman earthquake as obtained with a *P*-wave back-projection method for global seismic stations (left) and European stations only (right). The mainshock is the star at the plot origin; aftershock locations are shown as dots.

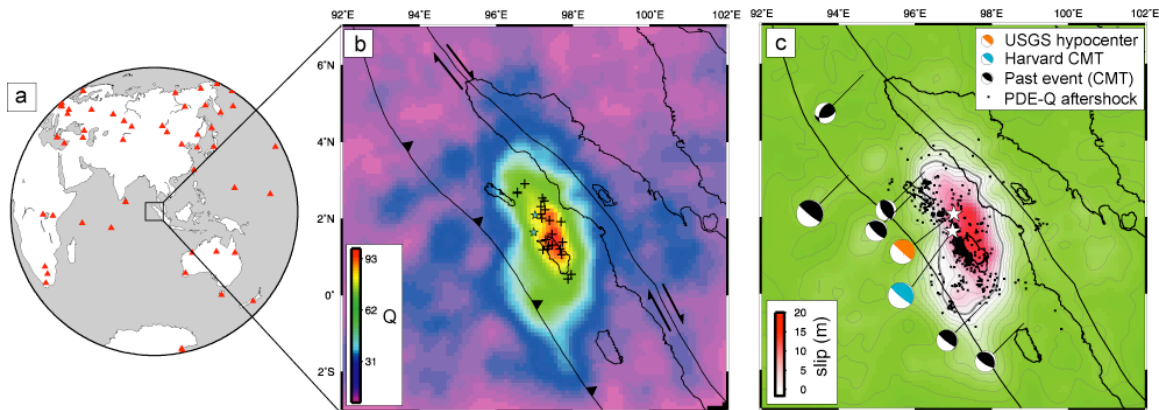


Figure 3. Images of back-projected *P*-wave energy for the March 28, 2005, $M_w = 8.7$ Sumatra earthquake. (a) The station distribution with respect to the epicenter. (b) Estimated relative seismic energy release with plus symbols showing spatial centroids at different times. (c) Estimated slip using a simple energy/moment scaling relationship. Aftershock locations and selected focal mechanisms are also plotted. The thick gray contour outlines our estimate of the fault plane.

We filtered *P* waves for this earthquake as recorded by GSN stations to between 2 and 30 s period. Initial *P*-wave arrivals are coherent among the stations except for those at azimuths near 250 degrees where there is a node in the *P*-wave radiation pattern. We aligned these traces in time using waveform cross-correlation on the first 15 s of the traces. Results of the back-projection method are shown in Figure 3. Our resulting image agrees favorably with the distribution of the aftershocks and the location of the Harvard central moment tensor. The back-projected energy suggests that the rupture proceeded from the hypocenter in two directions: for a short distance toward the north and a much longer distance to the south. The observed *P*-wave radiation throughout the rupture zone is characterized by frequencies between 0.5 and 0.1 Hz. However, the seismic radiation in the south half of the rupture zone also contains lower frequencies (0.03 to 0.1 Hz), perhaps suggesting either temporal changes in rupture velocity or stress drop during rupture.

References

- Earle, P.S. and P.M. Shearer, Characterization of global seismograms using an automatic picking algorithm, *Bull. Seismol. Soc. Am.*, **84**, 366–376, 1994.
- Ishii, M., P.M. Shearer, H. Houston and J.E. Vidale, Rupture extent, duration, and speed of the 2004 Sumatra-Andaman earthquake imaged by the Hi-Net array, *Nature*, doi:10.1038/nature03675, 2005.
- Ni, S., H. Kanamori and D. Helmberger, Energy radiation from the Sumatra earthquake, *Nature*, **434**, 582, 2005.
- Walker, K., P. Shearer, M. Ishii and P. Earle, Telesismic imaging of the rupture zone of the 28 March 2005 Sumatra Mw 8.7 earthquake, *Geophys. Res. Lett.*, in press, 2005.

Non-technical Summary

We are developing methods for imaging the rupture plane of large earthquakes using seismic arrivals at distant seismic stations. Our method can provide detailed information about the duration and rupture direction of these earthquakes, which should assist in the rapid calculation of strong ground-motion predictions.

Reports Published

- Ishii, M., P.M. Shearer, H. Houston and J.E. Vidale, Rupture extent, duration, and speed of the 2004 Sumatra-Andaman earthquake imaged by the Hi-Net array, *Nature*, doi:10.1038/nature03675, 2005.